# Understanding Microwave Heating in Biomass-Solvent Systems

Ali Taqi[1], Etienne Farcot[2], John P. Robinson[1], Eleanor R. Binner[1*]

[1]Faculty of Engineering, University of Nottingham, NG7 2RD, UK

[2]School of Mathematical Sciences, University of Nottingham, NG7 2RD, UK

*Corresponding author: eleanor.binner@nottingham.ac.uk

## Abstract

A new mechanism is proposed to provide a viable physical explanation for the action of microwaves in solvent extraction processes. The key innovation is Temperature-Induced Diffusion, a recently-demonstrated phenomenon that results from selective heating using microwaves. A mechanism is presented which incorporates microwave heating, cellular expansion, heat transfer and mass transfer, all of which affect the pressure of cell structures within biomass. The cell-pressure is modelled with time across a range of physical and process variables, and compared with the expected outputs from the existing steam-rupture theory. It is shown that steam-rupture is only possible at the extreme fringes of realistic physical parameters, but Temperature-Induced Diffusion is able to explain cell-rupture across a broad and realistic range of physical parameters and heating conditions. Temperature-Induced Diffusion is the main principle that governs microwave-assisted extraction, and this paves the way to being able to select processing conditions and feedstocks based solely on their physical properties.

## Graphical abstract

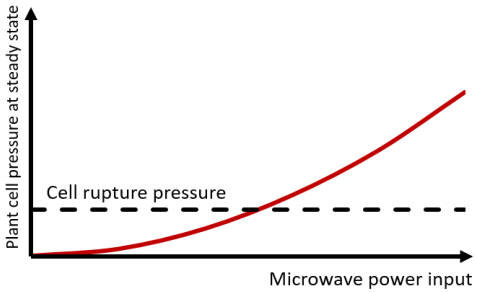


## Keywords

Microwave processing, heat transfer, mass transfer, plant cell rupture, cellular expansion mechanics, solvent extraction

## Nomenclature

| Symbols | | |
|---|---|---|
| **Symbol** | **Parameter** | **Unit** |
| | **Chemical potential** | |
| $\mu$ | Chemical potential | $Jmol^{-1}$ |
| $T$ | Temperature | ℃ |
| $\alpha$ | Activity | |
| $v$ | Specific volume | $m^3mol^{-1}$ |
| $s$ | Entropy | $Jmol^{-1}K^{-1}$ |
| $R$ | Universal gas constant | $Jmol^{-1}K^{-1}$ |
| $P$ | Pressure | $bar$ |
| | **Microwave heating and heat transfer** | |
| $t$ | Time | $s$ |
| $k$ | Thermal conductivity | $Wm^{-1}K^{-1}$ |
| $\beta$ | Heat transfer coefficient | $m^2s^{-1}$ |
| $F$ | Microwave frequency | $Hz$ |
| $\varepsilon_0$ | Permittivity of free space | $m^{-3}kg^{-1}s^4A^2$ |
| $\varepsilon''$ | Dielectric loss factor | |
| $\varepsilon''_{biomass}$ | Dielectric loss factor of the biomass | |
| $\varepsilon''_{solvent}$ | Dielectric loss factor of the solvent | |
| $\Delta\varepsilon''$ | Difference between the loss factors of biomass and solvent | |
| $E$ | Electric field intensity | $Vm^{-1}$ |
| $\Delta T_{max}$ | Maximum temperature difference between the biomass and the solvent phase at thermal steady state | ℃ |
| $\rho$ | Mass density | $kgm^{-3}$ |
| $D_p$ | Penetration depth | $m$ |
| $C_p$ | Specific heat capacity | $Jmol^{-1}K^{-1}$ |
| | **Cell expansion mechanics** | |
| $\sigma$ | Stress | $MPa$ |
| $\epsilon$ | Strain | |
| $Y$ | Elastic modulus at zero strain | $MPa$ |
| | **Mass transfer and cellular mechanics** | |
| $L$ | Mass transfer coefficient | $mol^2J^{-1}m^{-1}s^{-1}$ |
| $M$ | Molar quantity | $mol$ |
| $\delta V$ | Volume of a given phase | $m^3$ |
| $\alpha_{W0-cell}$ | Initial water activity in the cell | $barg$ |
| $D_{AB}$ | Fick's law diffusivity | $m^2s^{-1}$ |
| $P_{max}$ | Maximum biomass cell pressure at equilibrium | $bar$ |
| $t_{99}$ | Time required to achieve 99% of the equilibrium value | $s$ |

## Superscripts and subscripts

| Superscripts and subscripts | | |
|---|---|---|
| **Symbol** | **Significance** | **Example** |
| $()_i$ | Property of a component "i" | $\mu_i$; chemical potential of component "i" |
| $()^0$ | Parameter at the baseline/datum condition | $T^0$; baseline/datum temperature |
| $()_{i()}$ | Property of a component "i" at given condition(s) | $s_{i(T)}$; entropy of component "i" at temperature T |
| $()_L$ | Parameter of a condensed state | $v_L$; specific volume of the liquid state |
| $()_W$ | Property of the solvent component (i.e. water) | $s_{W(T^0)}$; entropy of water at the baseline/datum temperature |
| $()_{jkl}$ | Parameter at a given numerical position jkl | $\delta V_{jkl}$; volume of a numerical element at numerical position jkl |

## 1 Introduction

Biomass is an attractive alternative to fossil reserves for the production of fuels and platform chemicals [1]. This includes novel routes to platform chemicals using green chemistry and industrial biotechnology approaches [2], but also the extraction of bio-based chemicals with wide-ranging applications including in the pharmaceutical and health industries [3], and the production of functional materials (e.g. adsorbents) from solid residues [4]. The heterogeneity and recalcitrance of biomass materials limits the effectiveness of available processing technologies [5], so the development of novel processes and chemistry is required for large-scale processing to become economically viable.

Microwave processing has been widely reported to accelerate or enhance biomass-upgrading processes [6]. The unique ability of electromagnetic waves to transfer and dissipate energy volumetrically means that microwave processes can be fast, continuous, compact and flexible in operation. They can be portable, potentially operating on farms or food production sites, avoiding the major logistical challenge of transporting distributed feedstocks to a central processing facility, and minimising degradation during transport. Microwaves also heat selectively, which means that they heat different components of heterogeneous systems at different rates, and it is thought that this can lead to rupture of cells within biomass, resulting in higher extraction yields and the ability to treat recalcitrant lignocellulosic materials. Although there is widespread recognition of the potential benefits of microwave processes in the chemical and pharmaceutical sectors, the effects of the unique heating mechanisms on heat and mass transfer, chemical transformations and potential physical rupture of the plant material are poorly understood. It is this lack of mechanistic understanding that poses the major barrier to scale-up [7].

The currently-accepted theory is that microwaves promote rapid loosening of the cell wall matrix [8, 9] and cause cell rupture [10-12], and this alteration in the biomass microstructure enhances component extraction. To date, although many authors have discussed this phenomenon qualitatively, and some have illustrated structural changes in biomass using microscopic imaging [12-14], there is no clear evidence of how (and arguably if) microwave heating leads to structural modification of biomass. There have been two recent attempts to quantify this phenomenon. The first relates to the common hypothesis that rapid and internal heating by microwaves induces vaporisation within the cellular structures, thereby quickly increasing pressure and causing cell rupture [3, 15-22]. A quantitative model has been proposed by Chan et al. [23] to link microwave heating with cell pressure due to intracellular steam generation, which couples microwave heating, water vaporisation and mechanical cell wall properties to predict internal pressure and cell rupture time. The model correctly predicts a rupture time of the order of minutes, which is consistent with empirical observations, however conventional heat transfer is not

considered in this approach. Biomass heats selectively and attains a higher temperature than the surrounding solvent, however no consideration is made of the heat flow from biomass to solvent nor the steady state temperature that could result during microwave heating. The Chan model represents a major step towards a mechanism for microwave-assisted extraction but there are missing physical phenomena that need to be included and investigated over a realistic set of conditions before a quantitative assessment of steam-rupturing can be presented.

An alternative theory to explain plant cell disruption using microwaves has been proposed by Lee et al. [24]. The extraction of solutes from plant materials is characterised as a mass transfer process [16], involving (i) penetration of the solvent into the solid, (ii) solubilisation-desorption of the solute from the solid matrix and/or hydrolysis, (iii) diffusion to the surface of the biomass, and (iv) external transfer into the bulk solution. The Lee theory proposes that microwave selective heating can fundamentally change these mass transfer processes, and this could lead to disruption of the cellular structure. Solvents such as water flow between the cell and solvent phases down a chemical potential gradient until mass equilibrium is achieved. Chemical potential is a quantity that combines the different driving forces for mass transfer into a single mathematical expression [25]. These driving forces include gradients in pressure, temperature and component activity. Selective heating with microwaves induces temperature gradients between cells and the solvent phase in a biomass-solvent system. This phenomenon, which is absent in conventional heating, acts as an additional driving force for mass transfer. If the intracellular components are heated selectively over the solvent, the chemical potential of these intracellular components is reduced, and this leads to movement of the solvent into cells, inducing higher cell pressures. Liquids such as water are nearly incompressible, and if liquid flows into a cell there will be a subsequent pressure increase due to the resistance to expansion provided by the cell walls, a phenomenon which could lead to disruption of the cellular structure. Lee et al. [24] showed that a temperature difference of just 1 ℃ could potentially lead to equilibrium cell pressures exceeding 100 bar, which the authors stated would be sufficient to exceed the yield stress of most cellular structures. Furthermore, the theory that selective heating can drive mass transfer has recently been validated experimentally; reverse osmosis for water desalination was achieved without the need for the application of pressure as in conventional reverse osmosis processes [26]. Despite the novelty and step-change in understanding, the study by Lee et al. [24] was limited to steady-state, so it is not possible to assess whether the kinetics of Temperature-Induced Diffusion are within the same timeframe as empirical microwave extraction studies.

The aim of this work is to build on the theoretical approaches of Chan and Lee, adding heat transfer and mass transfer kinetics. This will determine whether temperatures high enough for intracellular steam generation can be achieved in the Chan approach, and if the mass transfer kinetics in the Lee model are within empirically-observed ranges, ultimately allowing an assessment of each model as a viable mechanism for microwave-assisted extraction. Two distinct methodologies are required, one for temperature and one for mass transfer.

## 2 Temperature distribution during microwave heating

This section presents the methodology and results when a heat transfer element is included with microwave heating of biomass-solvent systems. The temperature distributions established using this approach will subsequently be used to test the steam-rupture hypothesis, and to provide input parameters to investigate Temperature-Induced Diffusion.

### *2.1 Methodology*

#### *2.1.1 System Geometry*

Biomass cells were approximated as a cuboid, which resembles cell types such as onion epidermal cells [27-31] that are well characterised in terms of their mechanical behaviour [29-31]. Individual cells are 100 $\mu m$ length, 50 $\mu m$ width, 10 $\mu m$ height and 1 $\mu m$ wall thickness [27-31]. When multiple cells are considered, they are assumed to have an identical geometry and a regular arrangement, with their interior assumed to consist of an aqueous solution with defined activity. The amount of solvent surrounding a cell cluster is defined by a solvent to solid ratio of 100 *ml/g*.

#### *2.1.2 Heating Rate Equation*

Microwaves heat volumetrically due to energy dissipation as the electric field component interacts with the process material. The main mechanisms by which electromagnetic waves heat materials within the microwave frequency range are dipolar polarisation and ionic conduction [32]. The extent to which electromagnetic energy is converted to heat is governed by the dielectric loss factor ($\varepsilon''$), which varies with frequency and temperature [33]. As an extraction process advances the temperature of both biomass and solvent will increase due to a combination of microwave heating and conventional heat transfer (*EQUATION 1*). Both the solvent and the cell can be heated with microwaves, and the extent depends on the electric field intensity (*E*) and the dielectric loss factor ($\varepsilon''$) [34].

$$\frac{dT}{dt} = \beta \nabla^2(T) + \frac{\beta}{k}\, 2\pi F \varepsilon_0 \varepsilon'' E^2$$

*Equation 1: Heating rate equation containing volumetric heating and conventional Fourier terms. Refer to nomenclature.*

*E* is a function of the applied power and reactor geometry, and also varies as energy is dissipated throughout the process material. Microwave attentuation is accounted for in this work using Lambert's law [35], where the strength of the electric field decays within a material as the wave attenuates. Conduction occurs through the cellular structure, and convective heat transfer takes place from the outer surface of the cell structure to the surrounding solvent. A steady state exists when the rate of volumetric energy dissipation in the biomass equals the rate of heat transfer into the surrounding solvent. As this study focussed on ambient pressure extraction processes the surrounding solvent is assumed to attain a maximum temperature at its normal boiling point. Further energy transfer into the solvent results in vaporisation, rather than a temperature increase.

### *2.1.3 Numerical solution*

This work employs a finite-difference time domain (FDTD) method to solve the partial-differential equation governing heat (*EQUATION 1*). The model is split into finite numerical points in space aligned in a Cartesian fashion (*FIGURE 1*) and the heating rate equation is solved for each numerical point over a predefined time domain. The spatial second derivatives in temperature in *EQUATION 1* are approximated with a second-order Taylor series approximation. This gives *EQUATION 2* which is then solved for each numerical point over a defined time domain.

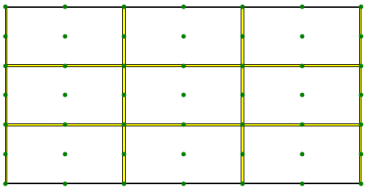

*Figure 1: XY plane showing a 3x3x3-cell system. Dots depict the solutions generated by the FDTD method.* ***(Colour required)***

$$\left.\frac{dT}{dt}\right|_{jkl} \approx 2\beta\left(\frac{T_{(j+1)kl}-2T_{jkl}+T_{(j-1)kl}}{\delta x_{(j+1)kl}{}^{2}+\delta x_{(j-1)kl}{}^{2}}+\frac{T_{j(k+1)l}-2T_{jkl}+T_{j(k-1)l}}{\delta y_{j(k+1)l}{}^{2}+\delta y_{j(k-1)l}{}^{2}}+\frac{T_{jk(l+1)}-2T_{jkl}+T_{jk(l-1)}}{\delta z_{jk(l+1)}{}^{2}+\delta z_{jk(l-1)}{}^{2}}\right)+\frac{\beta}{k}\,2\pi F\varepsilon_0\varepsilon''|E|^2$$

*Equation 2: Second-order Taylor series approximation of the heat equation.*

## *2.2 Predicted Temperature distribution*

*EQUATION 1* is solved for a range of input parameters to give a series of temperature-time relationships, which are the required output. Outputs are presented according to the key physical and process variables, which are the dielectric loss factor ($\varepsilon''$), electric field intensity ($E$), biomass size and thermal conductivity ($k$). A single independent parameter was varied, keeping all other parameters constant. *TABLE A1* (*APPENDIX A*) summarises the universal constants used for the heating rate (*EQUATION 1*), while *TABLE A2* (*APPENDIX A*) summarises the variables and constants for the different analyses conducted.

*2.2.1 Effect of Dielectric Loss Factor ($\varepsilon''_{biomass}$, $\varepsilon''_{solvent}$)*

The value of $\varepsilon''_{biomass}$ was fixed at 25, while $\varepsilon''_{solvent}$ was varied from 0 ($\Delta\varepsilon'' = 25$) to 50 ($\Delta\varepsilon'' = -25$). This is not intended to represent a particular physical condition, but will span the full range from a microwave-transparent solvent to one that absorbs much more strongly than the biomass itself. $k$ was fixed at $0.05\ Wm^{-1}K^{-1}$, $E$ was taken as 10000 $Vm^{-1}$ which the limit for single-mode microwave cavities [36], and the solvent was assumed to have a boiling point of 100 ℃. FIGURE 2 shows the temperature increase with time for both the solvent and a single cell for the two extreme cases of $\Delta\varepsilon''$. For simplicity, the solvent's temperature corresponds here to that of a numerical point at the edge of the cell cluster. In reality the solvent will only have a homogeneous temperature when at the boiling point.

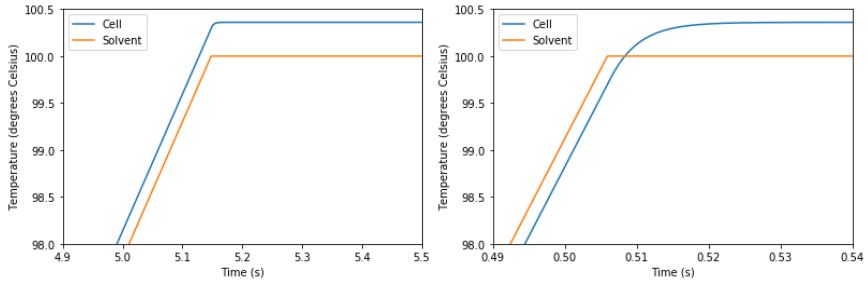


*Figure 2: Temperature for a single cell in solvent during microwave heating. (A) Microwave-transparent solvent - Δε"=25; (B) Microwave-absorbent solvent - Δε"=-25.* ***(Colour required)***

FIGURE 2A shows that the cell is at a higher temperature than the solvent during the heat-up period, which is to be expected given that the solvent is microwave-transparent, and only heats indirectly due to heat transfer from the cell. The solvent temperature plateaus at the boiling point (100°C) and the cell temperature continues to increase. The cell temperature plateaus shortly after the solvent temperature, which is due to thermal equilibrium between volumetric heating and heat transfer to the surrounding solvent. In FIGURE 2A the cell temperature is around 0.4°C higher than the surrounding solvent at thermal steady state under these physical conditions. For the microwave-absorbent solvent, FIGURE 2B shows that the solvent temperature is higher than the cell temperature during the heat-up period, which is to be expected given that the solvent absorbs more energy volumetrically than the biomass. The solvent attains its boiling point temperature in around 0.5 seconds in this case, compared to 5 seconds for the case of a microwave-transparent solvent. Whilst the solvent temperature is limited to the boiling point the same is not true for the cell, so although it absorbs less energy volumetrically than the solvent it can continue to heat beyond 100°C. In this case the cell temperature plateaus at around 100.4°C as a thermal steady state is reached, which is identical to the equilibrium temperature in FIGURE 2A. The outcomes shown in FIGURE 2 indicate

that the steady state temperature of a single cell of biomass is independent of the dielectric loss factor of the solvent, and always higher than that of the solvent given that the cell absorbs microwaves.

When multiple cells are considered there is a gradient in temperature, with a maximum in the centre of the cluster and a minimum at the biomass-solvent boundary. *FIGURE 3* shows an example of the temperature distribution at steady state for a biomass system consisting of 1000 cells, with $\varepsilon"_{biomass} = 20$ and $\varepsilon"_{solvent} = 5$. In this case the temperature difference between the centre of the cell cluster and the surrounding solvent is around 1 ℃. The maximum temperature difference between biomass and solvent at thermal steady state ($\Delta T_{max}$), for different-sized clusters and different values of dielectric loss factor of biomass and solvent, are summarised in ***ERROR! REFERENCE SOURCE NOT FOUND.***.

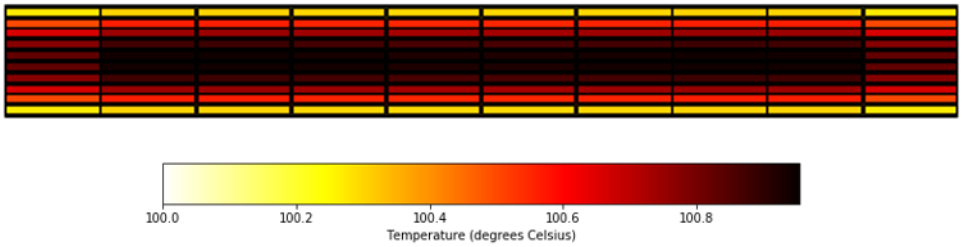


*Figure 3: Temperature distribution at thermal steady state for an XZ plane, $\varepsilon"_{biomass} = 20$; $\varepsilon"_{solvent} = 5$. $k = 0.6\ Wm^{-1}K^{-1}$, $E = 10000\ Vm^{-1}$.* ***(Colour required)***

| | | ***Number of cells*** | | |
|---|---|---|---|---|
| $\varepsilon"_{solvent}$ | $\varepsilon"_{biomass}$ | ***1*** | ***125*** | ***1000*** |
| ***5*** | ***0*** | *0.000* | *0.000* | *0.000* |
| | ***10*** | *0.012* | *0.143* | *0.477* |
| | ***20*** | *0.025* | *0.285* | *0.953* |
| | ***25*** | *0.031* | *0.357* | *1.192* |
| ***20*** | ***0*** | *0.000* | *0.000* | *0.000* |
| | ***10*** | *0.012* | *0.143* | *0.477* |
| | ***20*** | *0.025* | *0.285* | *0.953* |
| | ***25*** | *0.031* | *0.357* | *1.192* |

Table 1: Maximum temperature difference between biomass and solvent at thermal steady state ($\Delta T_{max}$) for variable dielectric loss factors and biomass geometry. k = 0.6 $Wm^{-1}K^{-1}$ and E = 10000 $Vm^{-1}$.

$\Delta T_{max}$ is a function of the size of the cell cluster and the dielectric loss factor of the biomass ($\varepsilon"_{biomass}$), but is independent of the dielectric loss factor of the solvent ($\varepsilon"_{solvent}$). In this case the largest $\Delta T_{max}$ was just 1.2°C for a 1000 cell cluster and biomass loss factor of 25. The biomass material will attain steady state temperatures that are higher than that of the solvent phase provided that $\varepsilon"_{biomass}$ is greater than zero.

*2.2.2 Effect of Electric Field Intensity (E)*

Electric field intensity (*E*) was varied at a constant *k* value of 0.6 $Wm^{-1}K^{-1}$, and for a case where the biomass heats selectively over the solvent; $\varepsilon"_{biomass}$ = 10, $\varepsilon"_{solvent}$ = 5. The maximum temperature difference between biomass and solvent at thermal steady state ($\Delta T_{max}$) is shown in

.

| | ***Number of cells*** | | |
|---|---|---|---|
| ***Electric Field Intensity*** $(Vm^{-1})$ | ***1*** | ***125*** | ***1000*** |
| ***0*** | *0.000* | *0.000* | *0.000* |
| ***2000*** | *0.001* | *0.006* | *0.019* |
| ***4000*** | *0.002* | *0.023* | *0.076* |
| ***6000*** | *0.005* | *0.051* | *0.172* |
| ***8000*** | *0.008* | *0.091* | *0.305* |
| ***10000*** | *0.012* | *0.143* | *0.477* |

Table 2: Maximum temperature difference between biomass and solvent at thermal steady state ($\Delta T_{max}$) for variable Electric field intensity (E) and biomass geometry. $\varepsilon"_{biomass}$ = 10, $\varepsilon"_{solvent}$ = 5, k = 0.6 $Wm^{-1}K^{-1}$. Solvent temperature is 100℃ and biomass temperature is higher.

It is shown in

that $\Delta T_{max}$ increases non-linearly with electric field intensity (*E*), with the effect being more pronounced for larger cell clusters. Higher *E* results in more volumetric energy dissipation within the biomass, and so higher temperature differences are required between the biomass and solvent phases to increase heat transfer into the solvent phase and achieve thermal steady state. When $E = 0\, Vm^{-1}$ no microwave power is applied, and hence the system resembles the case of conventional heating with no temperature differential between the biomass and the solvent.

*2.2.3 Effect of Thermal conductivity (k)*

Thermal conductivity was varied at a constant of *E*=10000 $Vm^{-1}$; $\varepsilon"_{biomass}$ = 10 and $\varepsilon"_{solvent}$ = 5. The maximum temperature difference between biomass and solvent at thermal steady state ($\Delta T_{max}$) is shown in *TABLE 3*.

| | ***Number of cells*** | | |
|---|---|---|---|
| ***Thermal Conductivity*** $(Wm^{-1}K^{-1})$ | ***1*** | ***125*** | ***1000*** |
| ***0.050*** | *0.144* | *1.655* | *5.526* |
| ***0.075*** | *0.096* | *1.103* | *3.686* |
| ***0.100*** | *0.072* | *0.827* | *2.764* |
| ***0.200*** | *0.036* | *0.414* | *1.382* |
| ***0.300*** | *0.024* | *0.276* | *0.922* |
| ***0.400*** | *0.018* | *0.207* | *0.691* |
| ***0.600*** | *0.012* | *0.143* | *0.477* |
| ***1.000*** | *0.007* | *0.083* | *0.276* |

Table 3: Maximum temperature difference between biomass and solvent at thermal steady state ($\Delta T_{max}$) for variable thermal conductivity (k) and biomass geometry. $\varepsilon"_{biomass}$ = 10, $\varepsilon"_{solvent}$ = 5, E = 10000 $Vm^{-1}$. Solvent temperature is 100℃ and biomass temperature is higher.

When thermal conductivity (*k*) is low there is more resistance to heat flow, so materials possessing very small *k* values are expected to attain much higher steady state temperatures than the solvent. In this case for a 1000-cell cluster a temperature difference of over 5.5°C is apparent when *k* = 0.05 $Wm^{-1}K^{-1}$, compared to just 0.28°C when *k* = 1.0 $Wm^{-1}K^{-1}$. Compared to *TABLE 1* the magnitude of the temperature variation in this case is much higher,

which indicates that thermal conductivity has a more dominant effect on equilibrium temerpature than the loss factor of either the biomass or the solvent.

### *2.3 Assessment of steam rupturing theory*

The enhanced understanding of heat flows and temperature during microwave processing can be used to evaluate the likelihood of intracellular steam generation. Using a similar approach to that shown in *TABLE 1* - *TABLE 3*, the physical and process parameters are investigated within ranges that are realistic for microwave-assisted extraction and biomass feedstocks. $E$ is fixed at 10000 $Vm^{-1}$, which the limit for single-mode microwave cavities [36]. The limit for $\varepsilon"_{biomass}$ is set at 35, as the largest reported $\varepsilon"_{biomass}$ is around 30 at 2.45 GHz [37]. The minimum limit for $k$ was set at 0.1 $Wm^{-1}K^{-1}$ as values as low as 0.2 have been reported for fruits and vegetables with 80% moisture [38]. The biomass geometry has been modified here to better resemble experimental situations. The number of cells in each dimension is defined so as to constitute a cube with dimensions ranging from 0.1 – 0.5 mm.

| | ***(A)*** $\boldsymbol{\varepsilon"_{biomass} = 35}$; ***Variable k*** $(\boldsymbol{Wm^{-1}K^{-1}})$ | | | ***(B)*** $\boldsymbol{k = 0.2\ Wm^{-1}K^{-1}}$; ***Variable*** $\boldsymbol{\varepsilon"_{biomass}}$ | | |
|---|---|---|---|---|---|---|
| ***Particle size (mm)*** | ***0.1*** | ***0.2*** | ***0.4*** | ***5*** | ***20*** | ***35*** |
| ***0.1*** | *5.4* | *2.7* | *1.3* | *0.4* | *1.5* | *2.7* |
| ***0.2*** | *17.1* | *8.6* | *4.3* | *1.2* | *4.9* | *8.6* |
| ***0.3*** | *34.4* | *17.2* | *8.6* | *2.5* | *9.8* | *17.2* |
| ***0.4*** | *56.8* | *28.4* | *14.2* | *4.1* | *16.2* | *28.4* |
| ***0.5*** | *83.8* | *42.0* | *21.0* | *6.0* | *24.0* | *42.0* |

Table 4: Maximum temperature difference between biomass and solvent at thermal steady state ($\Delta T_{max}$), for a realistic range of physical conditions and E = 10000 $Vm^{-1}$. Solvent temperature is 100℃ and biomass temperature is higher.

*TABLE 4* shows that the largest $\Delta T_{max}$ is around 84 ℃ and occurs under the extreme conditions of electric field intensity, particle size, thermal conductivity and loss factor. Under more realistic conditions it is likely that a temperature difference of just 10-20°C is achieved, and it should also be noted that the highest temperature will occur within the centre of the biomass, with lower temperatures towards the surface where it approaches the solvent temperature. For cell rupture to occur, the internal pressure must exceed the mechanical resistance of the cell walls. If the pressure is generated from steam created during microwave heating, then the boiling temperature must be consistent with the higher internal cell pressure. Under the most extreme conditions the maximum temperature that can occur within biomass during an ambient-pressure extraction process is 184 ℃ (i.e. the solvent temperature of 100 ℃ and temperature difference of 84 ℃). At 184°C the steam pressure equates to 10 atm, which is sufficient to cause rupture within some types of cell. However, away from the centre of the biomass and under realistic physical and processing conditions the temperature and pressure will be much lower. Cell rupture due to intracellular steam generation could therefore occur at the extreme fringes of physical and experimental

conditions, but it is highly unlikely to be as widespread as previously proposed. An alternative mechanism must exist for the generation of internal cell pressure during microwave heating.

## 3 Cell pressure during microwave heating

Lee et al. [24] were the first to highlight the possibility of Temperature-Induced Diffusion due to microwave heating. This section extends their initial work to encompass a realistic range of physical and heating conditions, and introduces mechanical and kinetic elements to understand the impact on cell pressure, and ultimately whether cell rupture can occur within the timeframes reported in empirical studies.

### *3.1 Methodology*

#### *3.1.1 Chemical potential and mass transfer*

The chemical potential of a component in a mixture is a universal property that dictates the direction and magnitude of the driving force for mass transfer. The chemical potential of a component "i" in a mixture at given temperature and pressure, and with fixed activity of the component "i", is expressed in ***EQUATION 3***. Refer to Robinson et al. [26] for derivation.

$$\mu_i = {\mu_i}^0 + v_L P_L - s_{i(T^0)}(T - T^0) + RTln\left(\frac{\alpha_i}{{\alpha^0}_i}\right)$$

*Equation 3: Chemical potential for variable pressure, temperature and activity. Refer to nomenclature.*

For water as the solvent the input parameters for the chemical potential expression are: ${\mu_W}^0 = 0\, Jmol^{-1}$, $T^0 = 25℃$; $s_{W(T^0)} = 70\, Jmol^{-1}K^{-1}$ [61] and ${\alpha^0}_W = 1$. If the system temperature is constant then the chemical potential expression becomes analogous to the classical osmotic pressure expression. If both the temperature and the pressure are constant, the spatial gradient of the chemical potential quantity reverts to an analogous form of Fick's law of diffusion. ***EQUATION 4*** is the expression governing mass transfer through the chemical potential analogy presented here.

$$\frac{dM_i}{dt} = L\delta V\nabla^2(\mu_i)$$

*Equation 4: Mass transfer equation. Refer to nomenclature.*

It is assumed that the biomass-solvent system contains two species: the solvent, which exists in pure form in the solvent phase and is able to diffuse into the cells, plus a solute which only exists within the cells. The rate-limiting step is assumed to be diffusion though the cell membrane, and component activity is assumed to equal molar concentration in this case (ideal mixture). The diffusion coefficient, $L$, is estimated from the molar diffusivity [25], which is taken as $10^{-12}\, m^2s^{-1}$ [39] and varied by an order of magnitude as part of a sensitivity analysis.

Solving the partial differential mass equation (*EQUATION 4*) requires a second-order Taylor series approximation (*EQUATION 5*), which is then solved numerically.

$$\left.\frac{dM}{dt}\right|_{jkl} \approx 2L\left(\frac{\mu_{(j+1)kl} - 2\mu_{jkl} + \mu_{(j-1)kl}}{\delta x_{(j+1)kl}{}^2 + \delta x_{(j-1)kl}{}^2} + \frac{\mu_{j(k+1)l} - 2\mu_{jkl} + \mu_{j(k-1)l}}{\delta y_{j(k+1)l}{}^2 + \delta y_{j(k-1)l}{}^2} + \frac{\mu_{jk(l+1)} - 2\mu_{jkl} + \mu_{jk(l-1)}}{\delta z_{jk(l+1)}{}^2 + \delta z_{jk(l-1)}{}^2}\right)\delta V_{jkl}$$

*Equation 5: Second-order Taylor series approximation of the mass equation. Refer to nomenclature.*

### *3.1.2 Cell Expansion*

Cells see an increase in pressure if mass influx of liquid takes place, or if the liquid density decreases due to an increase in temperature. The increase in pressure takes place due to the resistance to volumetric expansion provided by the rigid wall that surrounds each cell, with internal pressure directly related to stress in the cell wall. A cell wall fragment can be envisaged as a polymer constituted of cellulose microfibrils contained within an amorphous matrix [40-42]. Therefore, cell wall fragments are expected to exhibit mechanical behaviour similar to that of typical rubber materials, but with significantly higher elastic moduli due to the reinforcing components present. This has been supported experimentally for hydrated cell wall fragments of onion epidermis [31]. The stress-strain behaviour of a typical non-lignified cell wall fragment can be represented mathematically using an expression for rubber materials (*EQUATION 6*) [43] that is subsequently fitted to empirical data for biomass to yield the adjustable parameters.

$$\sigma/_W = (\,(1 + Z\epsilon)^{-1} - (1 + Z\epsilon)^{-2}\,) \exp 0.38(\,(1 + Z\epsilon) - (1 + Z\epsilon)^{-1})$$

*Equation 6: Stress-strain behaviour of typical non-lignified cell wall fragment. Refer to nomenclature.*

The parameters $W$ and $Z$ are manipulated to fit experimental stress-strain curves, with the additional constraint that their product is equal to $Y$, the elastic modulus of the fragment at zero strain. The value of $Y$ is taken as 800 *MPa* so as to reproduce experimental findings [31], and is varied as part of a sensitivity analysis (*TABLE A2*).

As solvent diffuses into the cell the volume expands, leading to a strain in the cell wall that can be calculated from the change in volume. The stress can then be calculated from *EQUATION 6* and used to infer cell pressure. It is assumed that cell expansion is accompanied by a reduction in the wall thickness [28, 40-42], and that cells will only experience strain in their largest dimension [29, 42]. A numerical analysis was conducted (*APPENDIX B*) to construct the cell pressure-volume relationship and thus define the cell expansion mechanics. This relationship is shown in (*FIGURE B1*), where a cell pressure value can be interpolated if its volumetric strain is known, and vice versa.

*3.1.3 Combining heat transfer, mass transfer and cell expansion*

The temperature gradient between cell and solvent calculated from EQUATION 1 provides an additional driving force for mass transfer between the biomass and the solvent phase, and this extra driving force is included within the chemical potential gradient (EQUATION 3). The mass transfer rate is subsequently calculated using EQUATION 4, which consequently changes the pressure within the cell (due to volumetric expansion) and the activity (due to dilution). As activity and pressure change the chemical potential gradient also changes, which in turn influences the mass transfer rate. The interdependence of the different parameters is illustrated in FIGURE 4. The novelty of this work is that it combines heat transfer, mass transfer and cell mechanics into a single mathematical framework, which is able to calculate cell temperature and pressures over time for clusters of cells.

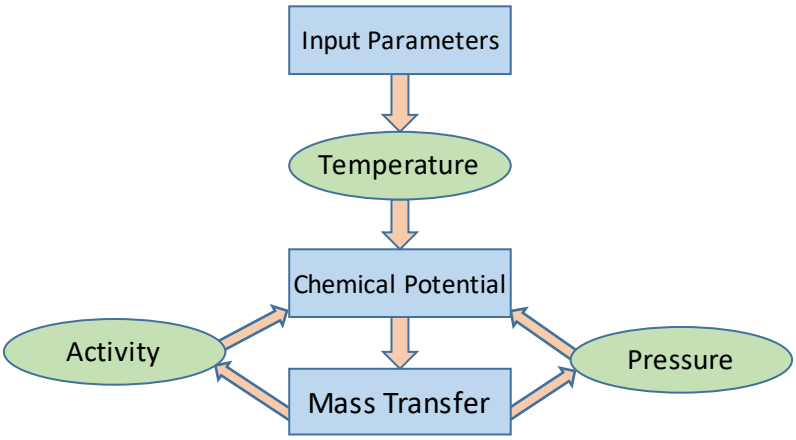


*Figure 4: Numerical computation framework.*

## *3.2 Predicted Pressure Distribution*

Cell pressure is a function of time, electric field intensity, dielectric properties, thermal conductivity, diffusivity, cell cluster size, elastic modulus and the solvent activity within the cell. The model outputs are presented in the first instance for variable process conditions with physical properties set at realistic values for biomass and solvent extraction. A sensitivity analysis is subsequently carried out to determine the effect of physical properties on cell pressure. TABLE A2 (APPENDIX A) summarises the variables and constants for the different analyses conducted.

*3.2.1 Effect of microwave heating parameters*

A biomass-solvent system consisting of a single cell was initially considered, with $E = 10000\ Vm^{-1}$, $k = 0.05\ Wm^{-1}K^{-1}$, $\varepsilon''_{biomass} = 35$ and $\varepsilon''_{solvent} = 5$. The resulting pressure is shown in FIGURE 5, along with the corresponding cell and solvent temperature.

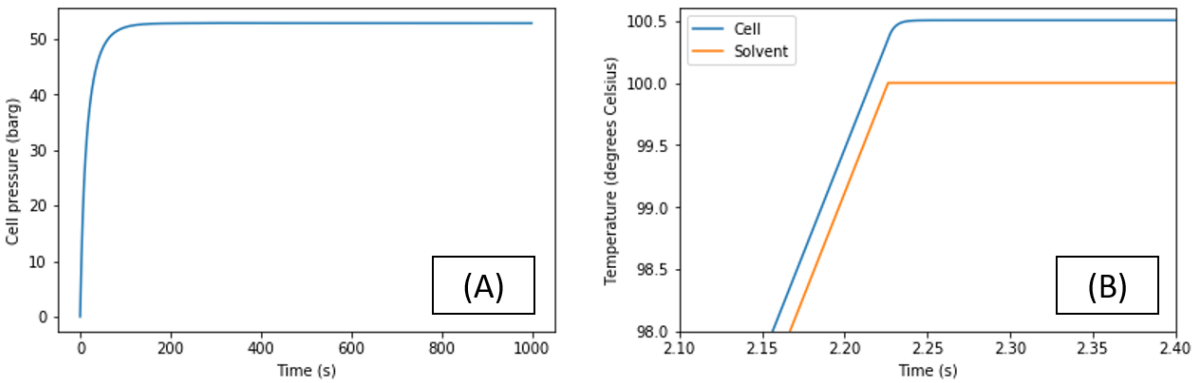


*Figure 5: Cell pressure with time and corresponding cell/solvent temperature* ***(Colour required)***

Under these conditions the cell pressure is induced during microwave heating rises to around 50 bar before appearing to reach equilibrium. The pressure build-up occurs in less than two minutes, which is well within the timeframe of numerous experimental microwave extraction studies [18, 20, 21, 24, 44-49].

It has been shown in section 2 that multicellular biomass materials exhibit a temperature distribution during microwave heating. Consequently, for clusters of cells a range of pressures are to be expected with a maximum around the centre of the cluster where the temperature is highest. FIGURE 6 illustrates an example of the pressure distribution at equilibrium when $E = 10000\, Vm^{-1}$, $k = 0.2\, Wm^{-1}K^{-1}$, $\varepsilon"_{biomass} = 10$ and the total particle size = 0.3 mm (30 x 6 x 3 cells).

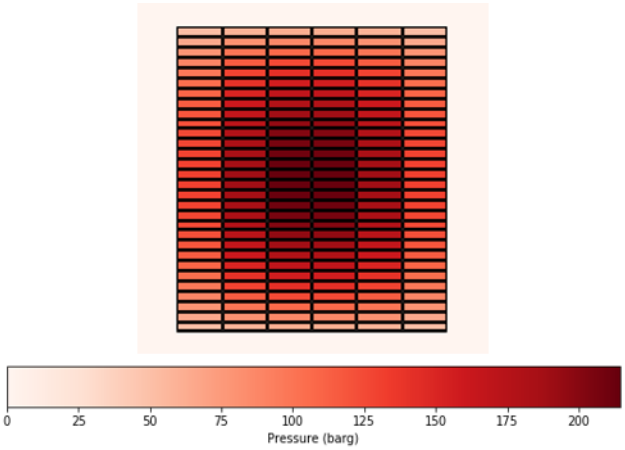


*Figure 6: Pressure distribution at equilibrium for a YZ plane.* $E = 10000\, Vm^{-1}$; $k = 0.2\, Wm^{-1}K^{-1}$, $\varepsilon"_{biomass} = 10$; *particle size = 0.3 mm.* ***(Colour required)***

For the cluster of 540 cells that comprise the 0.3mm particle the pressure within the centre cells is over 200 bar, whilst pressures on the outer edges of the cluster are still of the order of 50 bar. The pressure in this case is

primarily the result of the temperature that results from selective heating, and its subsequent effect on mass transfer and cell expansion. FIGURE 7 shows how the maximum pressure ($P_{max}$) within the cluster varies with both total particle size and the electric field intensity ($E$).

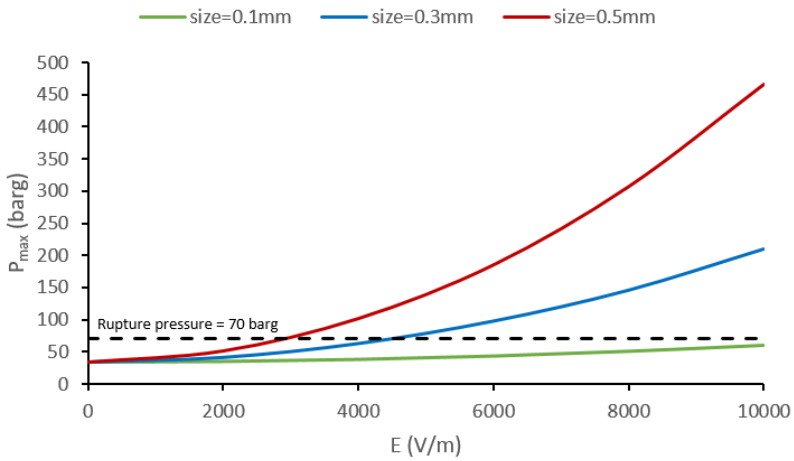


*Figure 7: Maximum equilibrium cell pressure against E for different biomass particle sizes. $k = 0.2\ Wm^{-1}K^{-1}$ and $\varepsilon''_{biomass} = 10$..* ***(Colour required)***

It is shown in FIGURE 7 that the maximum equilibrium pressure in a cell cluster ($P_{max}$) increases with both the cluster size and the electric field intensity ($E$). $P_{max}$ is more sensitive to $E$ with larger particles, indicating that while particles of all sizes see the same pressure profile under conventional heating (i.e. *E = 0 V/m),* they develop increasingly different pressure profiles according to their size and geometry as the input microwave power increases. FIGURE 7 includes a reference pressure of 70 bar as a rupture pressure for cells [24], and it is clearly evident that pressures beyond this threshold are entirely possible for a realistic range of particle size and $E$. When conventional heating is considered, i.e. the cell and solvent temperature both peak at 100°C, the cell pressure does not exceed 33.9 bar, which is well below the pressure needed for rupture in most cases. The cell pressure for a broader range of process conditions is shown in TABLE 5.

| | ***(A)*** $\boldsymbol{Particle\ size = 0.3\ mm;\ k = 0.2\ Wm^{-1}K^{-1};}$ ***Variable*** $\boldsymbol{\varepsilon''_{biomass}}$ | | | ***(B)*** $\boldsymbol{Particle\ size = 0.3\ mm;\ \varepsilon''_{biomass} = 10;}$ ***Variable k*** $\boldsymbol{(Wm^{-1}K^{-1})}$ | | | ***(C)*** $\boldsymbol{k = 0.2\ Wm^{-1}K^{-1};\ \varepsilon''_{biomass} = 10;}$ ***Variable particle size (mm)*** | | |
|---|---|---|---|---|---|---|---|---|---|
| $\boldsymbol{E\ (Vm^{-1})}$ | ***5*** | ***10*** | ***20*** | ***0.1*** | ***0.2*** | ***0.4*** | ***0.1*** | ***0.3*** | ***0.5*** |
| ***0*** | *33.9* | *33.9* | *33.9* | *33.9* | *33.9* | *33.9* | *33.9* | *33.9* | *33.9* |
| ***2000*** | *37.5* | *41.2* | *48.2* | *48.4* | *41.2* | *39.1* | *34.9* | *41.2* | *51.3* |
| ***4000*** | *48.2* | *62.8* | *89.9* | *90.9* | *62.8* | *50.2* | *38.0* | *62.8* | *101.6* |
| ***6000*** | *65.8* | *97.8* | *157.8* | *160.1* | *97.8* | *68.4* | *43.2* | *97.8* | *185.0* |
| ***8000*** | *89.9* | *146.1* | *257.1* | *257.1* | *146.1* | *93.2* | *50.3* | *146.1* | *306.9* |
| ***10000*** | *120.3* | *210.2* | *387.3* | *387.3* | *210.2* | *124.4* | *59.4* | *210.2* | *466.1* |

Table 5: Maximum cell pressure at mass equilibrium ($P_{max}$) for variable E, k, $\varepsilon"_{biomass}$ and particle size.

*TABLE 5* indicates a general increase in $P_{max}$ with higher values of $E$ under all process conditions. Furthermore, it is evident that $P_{max}$ increases with any change in the process conditions so as to increase $\Delta T_{max}$ (see section *2*). Hence, $P_{max}$ is more sensitive to $E$ when $\varepsilon"_{biomass}$ and particle size are larger, and when $k$ is smaller. It can be seen that, while the process conditions presented in *TABLE 5* are physically realistic, the differences between $P_{max}$ values are very large, with the smallest value of 33.9 bar occurring with conventional heating (i.e. $E = 0$ *V/m*), and the largest value of 466.1 bar occurring with $E = 10000$ *V/m*, $k = 0.2\ Wm^{-1}K^{-1}$, $\varepsilon"_{\text{biomass}} = 10$ and a particle size of *0.3 mm*. Considering 70 bar as a reference cell rupture pressure [24], it is clear again that pressures beyond this threshold are entirely possible for a realistic range of process conditions.

### *3.2.2 Sensitivity to physical properties*

The sensitivity of the maximum equilibrium cell pressure ($P_{max}$) to a secondary set of parameters was investigated. These were the initial cell water activity ($\alpha_{W0-cell}$), diffusivity ($D_{AB}$) and the elastic modulus of the cell at zero strain ($Y$). For this analysis the electric field intensity was set at 6000 *Vm*$^{-1}$, the thermal conductivity was 0.2 *Wm*$^{-1}$*K*$^{-1}$, $\varepsilon"_{\text{biomass}} = 10$ and particle size 0.3 *mm*.

| $\alpha_{W0-cell}$ | $P_{max}$ $(barg)$ |
|---|---|
| *0.97* | *111.1* |
| *0.98* | *97.8* |
| *0.99* | *83.2* |

Table 6: Maximum cell pressure at mass equilibrium ($P_{max}$) for variable $\alpha_{W0-cell}$.

| $Y$ $(MPa)$ | $P_{max}$ $(barg)$ |
|---|---|
| *250* | *88.2* |
| *400* | *91.4* |
| *600* | *95.2* |
| *800* | *97.8* |
| *1000* | *99.3* |
| *1500* | *100.8* |
| *2000* | *101.3* |
| *5000* | *101.9* |

*Table 7: Maximum cell pressure as mass equilibrium ($P_{max}$) for variable $Y$.*

| $D_{AB}$ $(m^2s^{-1})$ | $P_{max}$ $(barg)$ | $t_{99}(s)$ |
|---|---|---|
| $10^{-13}$ | *97.8* | *2890.0* |
| $10^{-12}$ | *97.8* | *289.0* |
| $10^{-11}$ | *97.8* | *28.9* |

Table 8: Maximum cell pressure at mass equilibrium ($P_{max}$) and time taken to approach 99% of this value ($t_{99}$), for variable $D_{AB}$.

The initial cell water activity ($\alpha_{W0-cell}$) was varied between 0.97 and 0.99, which is a realistic range for plant cell water activities [24]. The base value used in all previous analyses is 0.98. It can be seen in *TABLE 6* that $P_{max}$ increases as activity decreases, with a variation of around $\pm 15\ bar$ across the range of $\alpha_{W0-cell}$ investigated in

this case. This is because the lower activity implies a higher concentration of solute, which in turn increases the osmotic pressure of the cells.

On the other hand, the parameter $Y$ was varied between 250 MPa and 5000 MPa. The base value used in all previous analyses is 800 MPa, which matches experimental data on the elasticity of cell walls of onion epidermis [31] (*APPENDIX B*). *TABLE 7* shows the variation of $P_{max}$ with $Y$, where it is seen in this case that the maximum equilibrium pressure varies within around $\pm 7\ bar$ across the range of elastic modulus values tested. $P_{max}$ varies nonlinearly with $Y$, in that the sensitivity of $P_{max}$ to $Y$ becomes less pronounced as $Y$ increases. At low modulus values the cell tends to expand more readily upon water uptake. The increase in water content increases water activity, which in turn reduces the equilibrium pressure. At high modulus values the cell wall is much stiffer. In this case, less water uptake is needed to increase the pressure, and the water activity is lower than the case at low modulus values.

Diffusivity ($D_{AB}$) was varied by an order of magnitude and *TABLE 8* shows that there was no influence on the maximum equilibrium cell pressure ($P_{max}$). As it is a resistance term it does, however, influence the kinetics. *TABLE 8* shows the time required to attain a pressure that is 99% of the equilibrium value ($t_{99}$) when $D_{AB}$ is varied by an order of magnitude. It is seen that $t_{99}$ increases as $D_{AB}$ is decreased, and that it decreases as $D_{AB}$ is increased. While at $10^{-12}\ m^2 s^{-1}$ $t_{99}$ is equal to 289 seconds, an increase in $D_{AB}$ by an order of magnitude decreases $t_{99}$ to 28.9 seconds, and similarly a decrease in $D_{AB}$ by an order of magnitude increases $t_{99}$ to 2890 seconds.

### *3.3 Assessment of Temperature-Induced Diffusion for cell rupture*

The model results confirm that Temperature-Induced Diffusion can lead to pressures that are high enough to achieve cell rupture, even when the temperature difference between the biomass and the surrounding solvent is relatively small. High pressures can exist within a realistic timeframe, and with realistic values for electric field strength, dielectric loss factor, thermal conductivity and biomass particle/cell cluster size. The pressures do not show significant sensitivity to water activity or the elastic modulus of the cell wall. Diffusivity through the cell-cell wall boundary has a direct effect on the kinetics of the pressure increase, but not the equilibrium value, and across a realistic range of diffusivity values the time required for the cell pressures to increase is consistent with the duration of empirical studies carried out by numerous different researchers.

Further developments will be introduced to this model to make it applicable to wider range of experimental settings. For instance, it is important to remove the current restriction on solvent choice which in this work can only be high-purity water. Furthermore, future iterations of this predictive tool should consider extracts originating from the cell wall rather than the cell only. Hence, it is required to consider the cell wall as a distinct phase in

which the kinetics of water and solute flow and the kinetics of desorption from the cell wall are characterised. Also, the rates of solute generation within the cell wall should be considered, given that according to recent literature microwave heating is capable of enhancing reaction speeds [50] and overcoming some reaction rate-limiting steps constituted under conventional heating [51]. This work is intended as a first step towards a broader predictive tool that combines both theoretical and experimental approaches.

## 4 Conclusion

A new model was developed to describe the action of microwave heating on biomass-solvent systems, which includes microwave volumetric heating, heat transfer, mass transfer and cellular expansion mechanics. The model explains how temperature gradients arise within clusters of cells due to competing effects of volumetric heating and conventional heat transfer. Electric field strength, dielectric loss factor, thermal conductivity and the number of cells were all found to affect the internal cell temperature. However, in all but the most extreme of cases the magntidue of the temperature difference obtained under microwave heating was less than 40 ℃, which is not sufficient to underpin the steam-rupturing hypothesis. The multitude of empirical observations of cell rupture during microwave heating are therefore caused by another mechanism. The model was applied to the alternative hypothesis of Temperature-Induced Diffusion that was introduced by Lee et al. [24]. The kinetics of the pressure increase due to Temperature-Induced Diffusion are of the order of minutes, well-within the timeframes of empirical observations; pressures >70 bar can readily occur, which are high enough to cause cell rupture. It was found that pressures needed to cause cell rupture could be readily achieved within a range of processing conditions that are consistent with previous laboratory studies, and that there was little sensitivty to changes in initial water activity, diffusion coefficient and elastic modulus. The Temperature-Induced Diffusion model developed here provides a significant advance in the mechanistic understanding of microwave heating and mass transfer within biomass, and for the first time allows an experimentally-observed phenomenon to be rationalised with a realistic set of physical parameters. Further work will combine theoretical and experimental approaches to develop this new model into a broader predictive tool that can determine the suitability of different biomass feedstocks for microwave extraction processes based on widely available physical properties.

## Acknowledgements

This work was supported by the Engineering and Physical Science Research Council [grant number EP/R023948/1].

## Appendix A: Variables and input parameters

| *Parameter* | *Value* |
|---|---|
| $\beta = {}^{k}/_{\rho_L C_p}$ | *Depends on* $k, C_p$ *and* $\rho_L$ |
| $\rho_L = {}^{1}/_{v_l}$ | *Depends on temperature. Water data [52]* |
| $C_p$ | $4.182\ Jg^{-1}K^{-1}$ *[53]* |
| $F$ | $2.45\ GHz$ |
| $\varepsilon_0$ | $8.854 \times 10^{-12} m^{-3} kg^{-1} s^4 A^2$ |
| $D_p$ | *1 cm; typical order of magnitude for water [32]* |

*Table A1: Input parameters to the heat equations (*EQUATION 1*).*

| ***Figure/ Table*** | ***Parameter*** | | | | | | | |
|---|---|---|---|---|---|---|---|---|
| | ***Particle/ cell cluster size*** | $\varepsilon''_{biomass}$ | $\varepsilon''_{solvent}$ | $k$ $(Wm^{-1}K^{-1})$ | $E$ $(Vm^{-1})$ | $\alpha_{W0-cell}$ | $D_{AB}$ $(m^2s^{-1})$ | $Y$ $(MPa)$ |
| FIGURE 2*A* | *1 cell* | *25* | *0* | *0.05* | *10000* | *N/A* | *N/A* | *N/A* |
| FIGURE 2*B* | *1 cell* | *25* | *50* | *0.05* | *10000* | *N/A* | *N/A* | *N/A* |
| FIGURE 3 | *1000 (10x10x10) cells* | *20* | *5* | *0.6* | *10000* | *N/A* | *N/A* | *N/A* |
| TABLE 1 | *1, 125 (5x5x5), 1000 (10x10x10) cells* | *0, 10, 20, 25* | *5, 20* | *0.6* | *10000* | *N/A* | *N/A* | *N/A* |
| TABLE 2 | *1, 125 (5x5x5), 1000 (10x10x10) cells* | *10* | *5* | *0.6* | *0-10000* | *N/A* | *N/A* | *N/A* |
| TABLE 4*A* | *0.1-0.5 mm* | *35* | *5* | *0.1, 0.2, 0.4* | *10000* | *N/A* | *N/A* | *N/A* |
| TABLE 4*B* | *0.1-0.5 mm* | *5, 20, 35* | *5* | *0.2* | *10000* | *N/A* | *N/A* | *N/A* |
| FIGURE 5 | *1 cell* | *35* | *5* | *0.05* | *10000* | *0.98* | $10^{-12}$ | *800* |
| FIGURE 6 | *0.3 mm* | *10* | *5* | *0.2* | *10000* | *0.98* | $10^{-12}$ | *800* |
| FIGURE 7 | *0.1, 0.3, 0.5 mm* | *10* | *5* | *0.2* | *0-10000* | *0.98* | $10^{-12}$ | *800* |
| TABLE 5*A* | *0.3 mm* | *5, 10, 20* | *5* | *0.2* | *0-10000* | *0.98* | $10^{-12}$ | *800* |
| TABLE 5*B* | *0.3 mm* | *10* | *5* | *0.1, 0.2, 0.4* | *0-10000* | *0.98* | $10^{-12}$ | *800* |
| TABLE 5*C* | *0.1, 0.3, 0.5 mm* | *10* | *5* | *0.2* | *0-10000* | *0.98* | $10^{-12}$ | *800* |
| TABLE 6 | *0.3 mm* | *10* | *5* | *0.2* | *6000* | *0.97-0.99* | $10^{-12}$ | *800* |
| TABLE 7 | *0.3 mm* | *10* | *5* | *0.2* | *6000* | *0.98* | $10^{-12}$ | *250-5000* |
| TABLE 8 | *0.3 mm* | *10* | *5* | *0.2* | *6000* | *0.98* | $10^{-13}, 10^{-12}, 10^{-11}$ | *800* |

*Table A2: Value assignment for the different analyses.*

## Appendix B: Cell pressure-volume relationship

The cell pressure-volume relationship has been determined numerically, by defining an input cell pressure array with small increments and computing the stress (by Newton's third law), strain (using *EQUATION 6)* and cell volume for each pressure value in a stepwise manner. An initial condition was defined where the cell incorporates a known set of input geometry, atmospheric pressure and zero stress and strain in the cell wall. A base value of the elastic modulus at zero strain ($Y$) was taken as 80*0 MPa*, which reproduces experimental stress-strain curves reported for hydrated cell wall fragments of onion epidermis [31]. *FIGURE B1* shows cell pressure-volume relationship.

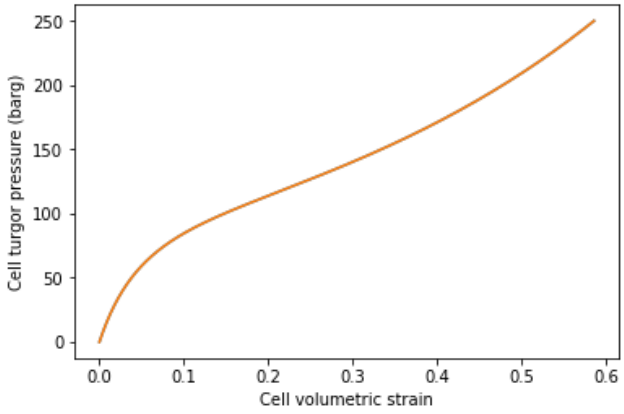


*Figure B1*: Cell pressure-volume relationship.

## References


[1] D. Beneroso, T. Monti, E. Kostas, and J. Robinson, "Microwave pyrolysis of biomass for bio-oil production: Scalable processing concepts," *Chemical Engineering Journal,* vol. 316, pp. 481-498, 2017.

[2] E4tech, *UK Top Bio-based Chemicals Opportunities*. London, 2017.

[3] N. Rombaut, A.-S. Tixier, A. Bily, and F. Chemat, "Green extraction processes of natural products as tools for biorefinery," *Biofuels, Bioproducts and Biorefining,* vol. 8, no. 4, pp. 530-544, 2014.

[4] X. Hu and M. Gholizadeh, "Biomass pyrolysis: A review of the process development and challenges from initial researches up to the commercialisation stage," *Journal of Energy Chemistry,* 2019.

[5] L. J. Douglas, "Conversion of Lignocellulosic Biomass to Ethanol," in *Energy applications of biomass*, M. Z. Lowenstein, Ed.: CRC Press, 2003.

[6] L. R. Adetunji, A. Adekunle, V. Orsat, and V. Raghavan, "Advances in the pectin production process using novel extraction techniques: A review," *Food Hydrocolloids,* vol. 62, pp. 239-250, 2017.

[7] W. J. Watson, "How do the fine chemical, pharmaceutical, and related industries approach green chemistry and sustainability?," *Green Chemistry,* vol. 14, no. 2, pp. 251-259, 2012.

[8] D. P. Leão, B. G. Botelho, L. S. Oliveira, and A. S. Franca, "Potential of pequi ( Caryocar brasiliense Camb.) peels as sources of highly esterified pectins obtained by microwave assisted extraction," *LWT - Food Science and Technology,* vol. 87, pp. 575-580, 2018.

[9] J. P. Maran and K. A. Prakash, "Process variables influence on microwave assisted extraction of pectin from waste Carcia papaya L. peel," *Int J Biol Macromol,* vol. 73, pp. 202-6, Feb 2015.

[10] F. Chemat and G. Cravotto, *Microwave-assisted extraction for bioactive compounds*. Springer, 2013, p. 240.

[11] S. C. Mandal, V. Mandal, and A. K. Das, *Essentials of botanical extraction: principles and applications*. Academic Press, 2015.

[12] T. M. Osaili, "Developments in the Thermal Processing of Food," in *Progress in food preservation*, R. Bhat, A. K. Alias, and G. Paliyath, Eds.: Wiley-Blackwell, 2012, pp. 211-230.

[13] F. Chemat and G. Cravotto, *Microwave-assisted extraction for bioactive compounds: theory and practice*. Springer Science & Business Media, 2012.

[14] S. C. Mandal, V. Mandal, and A. K. Das, "Classification of Extraction Methods," in *Essentials of Botanical Extraction*, S. C. Mandal;, V. Mandal;, and A. K. Das, Eds. Boston: Academic Press, 2015, pp. 83-136.

[15] M. A. Ferhat, B. Y. Meklati, J. Smadja, and F. Chemat, "An improved microwave Clevenger apparatus for distillation of essential oils from orange peel," *J Chromatogr A,* vol. 1112, no. 1-2, pp. 121-6, Apr 21 2006.

[16] N. Flórez, E. Conde, and H. Domínguez, "Microwave assisted water extraction of plant compounds," *Journal of Chemical Technology & Biotechnology,* vol. 90, no. 4, pp. 590-607, 2015.

[17] F. Guo, Z. Fang, C. C. Xu, and R. L. Smith Jr, "Solid acid mediated hydrolysis of biomass for producing biofuels," *Progress in Energy and Combustion Science,* vol. 38, no. 5, pp. 672-690, 2012.

[18] M. Kratchanova, E. Pavlova, and I. Panchev, "The effect of microwave heating of fresh orange peels on the fruit tissue and quality of extracted pectin," *Carbohydrate Polymers,* vol. 56, no. 2, pp. 181-185, 2004.

[19] R. M. Rodriguez-Jasso, S. I. Mussatto, L. Pastrana, C. N. Aguilar, and J. A. Teixeira, "Microwave-assisted extraction of sulfated polysaccharides (fucoidan) from brown seaweed," *Carbohydrate Polymers,* vol. 86, no. 3, pp. 1137-1144, 2011.

[20] M.-M. Yan, W. Liu, Y.-J. Fu, Y.-G. Zu, C.-Y. Chen, and M. Luo, "Optimisation of the microwave-assisted extraction process for four main astragalosides in Radix Astragali," *Food Chemistry,* vol. 119, no. 4, pp. 1663-1670, 2010.

[21] S. Yeoh, J. Shi, and T. A. G. Langrish, "Comparisons between different techniques for water-based extraction of pectin from orange peels," *Desalination,* vol. 218, no. 1-3, pp. 229-237, 2008.

[22] L. Zhongdong, W. Guohua, G. Yunchang, and J. F. Kennedy, "Image study of pectin extraction from orange skin assisted by microwave," *Carbohydrate Polymers,* vol. 64, no. 4, pp. 548-552, 2006.

[23] C.-H. Chan, H. K. Yeoh, R. Yusoff, and G. C. Ngoh, "A first-principles model for plant cell rupture in microwave-assisted extraction of bioactive compounds," *Journal of Food Engineering,* vol. 188, pp. 98-107, 2016.

[24] C. S. Lee, E. Binner, C. Winkworth-Smith, R. John, R. Gomes, and J. Robinson, "Enhancing natural product extraction and mass transfer using selective microwave heating," *Chemical Engineering Science,* vol. 149, pp. 97-103, 2016.

[25] J. G. Wijmans and R. W. Baker, "The solution-diffusion model: a review," *Journal of membrane science,* vol. 107, no. 1-2, pp. 1-21, 1995.

[26] J. Robinson, J. Meehan, A. Taqi, E. Binner, and B. Tokay, "Water desalination using a temperature gradient," *Desalination*, vol. 464, pp. 1-7, 2019.
[27] P. M. Pieczywek and A. Zdunek, "Finite element modelling of the mechanical behaviour of onion epidermis with incorporation of nonlinear properties of cell walls and real tissue geometry," *Journal of Food Engineering*, vol. 123, pp. 50-59, 2014.
[28] M. Shafayet Zamil, H. Yi, and V. M. Puri, "A multiscale FEA framework for bridging cell-wall to tissue-scale mechanical properties: the contributions of middle lamella interface and cell shape," *Journal of Materials Science*, vol. 52, no. 13, pp. 7947-7968, 2017.
[29] M. S. Zamil, H. Yi, M. A. Haque, and V. M. Puri, "Characterizing microscale biological samples under tensile loading: stress-strain behavior of cell wall fragment of onion outer epidermis," *Am J Bot*, vol. 100, no. 6, pp. 1105-15, Jun 2013.
[30] M. S. Zamil, H. Yi, and V. M. Puri, "Mechanical characterization of outer epidermal middle lamella of onion under tensile loading," *Am J Bot*, vol. 101, no. 5, pp. 778-87, May 2014.
[31] M. S. Zamil, H. Yi, and V. M. Puri, "The mechanical properties of plant cell walls soft material at the subcellular scale: the implications of water and of the intercellular boundaries," *Journal of Materials Science*, vol. 50, no. 20, pp. 6608-6623, 2015.
[32] A. a. Metaxas and R. J. Meredith, *Industrial microwave heating* (no. 4). IET, 1983.
[33] T. V. C. T. Chan and H. C. Reader, *Understanding microwave heating cavities*. Artech House Publishers, 2000.
[34] R. J. Meredith, *Engineers' handbook of industrial microwave heating* (no. 25). Iet, 1998.
[35] K. Ayappa, H. Davis, G. Crapiste, E. Davis, and J. Gordon, "Microwave heating: an evaluation of power formulations," *Chemical engineering science*, vol. 46, no. 4, pp. 1005-1016, 1991.
[36] J. Robinson *et al.*, "Understanding microwave heating effects in single mode type cavities—theory and experiment," *Physical Chemistry Chemical Physics*, vol. 12, no. 18, pp. 4750-4758, 2010.
[37] O. Sipahioglu and S. Barringer, "Dielectric properties of vegetables and fruits as a function of temperature, ash, and moisture content," *Journal of food science*, vol. 68, no. 1, pp. 234-239, 2003.
[38] P. Nesvadba, "Thermal properties of foods," in *Engineering properties of foods*, M. A. Rao, S. S. H. Rizvi, and A. K. Datta, Eds.: CRC press, 2005.
[39] G. D. Saravacos, "Mass transfer properties of foods," in *Engineering properties of foods*, M. A. Rao, S. S. H. Rizvi, and A. K. Datta, Eds.: CRC press, 2005.
[40] M. A. Chaplain, "The strain energy function of an ideal plant cell wall," *Journal of theoretical biology*, vol. 163, no. 1, pp. 77-97, 1993.
[41] H. I. WU, R. D. Spence, P. J. Sharpe, and J. D. Goeschl, "Cell wall elasticity: I. A critique of the bulk elastic modulus approach and an analysis using polymer elastic principles," *Plant, cell & environment*, vol. 8, no. 8, pp. 563-570, 1985.
[42] H.-i. Wu, R. D. Spence, and P. J. Sharpe, "Plant cell wall elasticity II: polymer elastic properties of the microfibrils," *Journal of theoretical biology*, vol. 133, no. 2, pp. 239-253, 1988.
[43] L. A. Wood, "Uniaxial Extension and Compression in Stress-Strain Relations of Rubber," *J. Res. Nat. Bur. Stand*, pp. 57-63, 1977.
[44] H. Bagherian, F. Zokaee Ashtiani, A. Fouladitajar, and M. Mohtashamy, "Comparisons between conventional, microwave- and ultrasound-assisted methods for extraction of pectin from grapefruit," *Chemical Engineering and Processing: Process Intensification*, vol. 50, no. 11-12, pp. 1237-1243, 2011.
[45] A.-M. Galan *et al.*, "New insights into the role of selective and volumetric heating during microwave extraction: Investigation of the extraction of polyphenolic compounds from sea buckthorn leaves using microwave-assisted extraction and conventional solvent extraction," *Chemical Engineering and Processing: Process Intensification*, vol. 116, pp. 29-39, 2017.
[46] I. T. Karabegović, S. S. Stojičević, D. T. Veličković, N. Č. Nikolić, and M. L. Lazić, "Optimization of microwave-assisted extraction and characterization of phenolic compounds in cherry laurel (Prunus laurocerasus) leaves," *Separation and Purification Technology*, vol. 120, pp. 429-436, 2013.
[47] J. Liu, R. Takada, S. Karita, T. Watanabe, Y. Honda, and T. Watanabe, "Microwave-assisted pretreatment of recalcitrant softwood in aqueous glycerol," *Bioresource technology*, vol. 101, no. 23, pp. 9355-9360, 2010.
[48] S. M. Nomanbhay, R. Hussain, and K. Palanisamy, "Microwave-Assisted Alkaline Pretreatment and Microwave Assisted Enzymatic Saccharification of Oil Palm Empty Fruit Bunch Fiber for Enhanced Fermentable Sugar Yield," *Journal of Sustainable Bioenergy Systems*, vol. 03, no. 01, pp. 7-17, 2013.
[49] S. Tsubaki, M. Sakamoto, and J.-i. Azuma, "Microwave-assisted extraction of phenolic compounds from tea residues under autohydrolytic conditions," *Food Chemistry*, vol. 123, no. 4, pp. 1255-1258, 2010.
[50] R. Wei, P. Wang, G. Zhang, N. Wang, and T. Zheng, "Microwave-responsive catalysts for wastewater treatment: A review," *Chemical Engineering Journal*, p. 122781, 2019.

[51] A. Amini, K.-i. Ohno, T. Maeda, and K. Kunitomo, "A kinetic comparison between microwave heating and conventional heating of FeS-CaO mixture during hydrogen-reduction," *Chemical Engineering Journal*, vol. 374, pp. 648-657, 2019.

[52] NIST. (2017, 24/09/2018). *Thermophysical Properties of Fluid Systems*. Available: https://webbook.nist.gov/chemistry/fluid/

[53] EngineeringToolbox. (2017, 24/09/2018). *Standard enthalpy of formation, Gibbs energy of formation, entropy and molar heat capacity of organic substances.* Available: https://www.engineeringtoolbox.com/standard-enthalpy-formation-value-Gibbs-free-energy-entropy-heat-capacity-organic-d_1979.html